A new method for depth of interaction determination in PET detectors

Pizzichemi, Marco; Stringhini, Gianluca; Niknejad, Tahereh; Liu, Zile; Lecoq, Paul; Tavernier, Stefaan; Varela, J; Paganoni, M; Auffray, Etiennette

Published in:
Physics in Medicine and Biology

DOI:
10.1088/0031-9155/61/12/4679

Publication date:
2016

Document Version:
Final published version

A new method for depth of interaction determination in PET detectors

Article *in* Physics in Medicine and Biology · June 2016

DOI: 10.1088/0031-9155/61/12/4679

9 authors, including:

Marco Pizzichemi
CERN
30 PUBLICATIONS **164** CITATIONS
SEE PROFILE

Gianluca Stringhini
CERN
5 PUBLICATIONS **13** CITATIONS
SEE PROFILE

Tahereh Niknejad
Laboratory of Instrumentation and Experime…
10 PUBLICATIONS **14** CITATIONS
SEE PROFILE

Zile Liu
University of Reading
113 PUBLICATIONS **175** CITATIONS
SEE PROFILE

IOP Publishing | Institute of Physics and Engineering in Medicine Physics in Medicine & Biology

Phys. Med. Biol. **61** (2016) 4679–4698 doi:10.1088/0031-9155/61/12/4679

A new method for depth of interaction determination in PET detectors

M Pizzichemi[1], G Stringhini[1,2], T Niknejad[3], Z Liu[1], P Lecoq[2], S Tavernier[3,4], J Varela[3], M Paganoni[1] and E Auffray[2]

[1] University of Milano-Bicocca, Milano, Italy
[2] CERN, Geneve, Switzerland
[3] Laboratorio de Instrumentacao e Fisica Experimental de Particulas, Portugal
[4] Vrije Universiteit Brussel, Ixelles, Belgium

E-mail: marco.pizzichemi@cern.ch

Received 15 January 2016, revised 26 March 2016
Accepted for publication 3 May 2016
Published 1 June 2016

Abstract

A new method for obtaining depth of interaction (DOI) information in PET detectors is presented in this study, based on sharing and redirection of scintillation light among multiple detectors, together with attenuation of light over the length of the crystals. The aim is to obtain continuous DOI encoding with single side readout, and at the same time without the need for one-to-one coupling between scintillators and detectors, allowing the development of a PET scanner with good spatial, energy and timing resolutions while keeping the complexity of the system low. A prototype module has been produced and characterized to test the proposed method, coupling a LYSO scintillator matrix to a commercial SiPMs array. Excellent crystal separation is obtained for all the scintillators in the array, light loss due to depolishing is found to be negligible, energy resolution is shown to be on average 12.7% FWHM. The mean DOI resolution achieved is 4.1 mm FWHM on a 15 mm long crystal and preliminary coincidence time resolution was estimated in 353 ps FWHM.

Keywords: depth of interaction, SiPM, LYSO, positron emission tomography

(Some figures may appear in colour only in the online journal)

1. Introduction

Positron emission tomography (PET) involves the use of particle detectors to identify pairs of 511 KeV gamma rays emitted by the annihilation process of a positron with an electron. PET modules consist in fast and bright scintillators, such as LYSO:Ce, coupled in various

geometries to photosensors, like photomultipliers tubes (PMTs) or silicon photomultipliers (SiPMs). Early detection of metabolic anomalies in human bodies, as well as pre-clinical research, require at the same time excellent performances in terms of spatial resolution and sensitivity.

Multipixel PET scanners attempt to achieve high level of spatial resolution by reducing the transverse dimensions of the scintillators, which can greatly increase the number of detector readout channels, especially if a one-to-one coupling between crystals and detectors is adopted. This results in increased system complexity and higher production costs.

Sensitivity can be improved by the use of long scintillators. While this effectively increases the interaction probability of the gamma rays crossing the crystals, it also introduces higher uncertainties on the real position of interaction of the incident particle. The spatial resolution of the scanner can therefore be deteriorated by parallax errors, particularly for devices imaging small volumes, as it is the case both for organ dedicated and small animal PETs. Various DOI encoding techniques have been proposed in literature in order to overcome this issue. Some examples include, among the others, independent readout of multiple layers of crystals (Levin 2002), pulse-shape discrimination schemes (Karp and Daube-Witherspoon 1987, Wiener *et al* 2013), detectors with light sharing DOI encoding (Miyaoka *et al* 1998, Liu *et al* 2001, Yang *et al* 2009, Ito *et al* 2010, 2013), double side readout methods (Bugalho *et al* 2009), phosphor coated scintillators (Berg *et al* 2016) and double side G-APD cross-strip readout (Kolb *et al* 2014).

Furthermore, the long aspect ratio of crystals increases the spread in photon propagation times inside the scintillator, leading to degradations of the overall timing resolution in PET scanners. However, it has been demonstrated that the DOI information extracted with the use of double side readout schemes can be used to mitigate the impact of photon propagation time jitter and improve the timing resolution of TOF-PET detectors (Kang *et al* 2015, Seifert and Schaart 2015).

In this paper we propose a new method to obtain depth of interaction information in a highly segmented scintillator array with single side readout, by keeping excellent crystal identification and good energy and timing resolution without the need for one-to-one coupling between crystals and detectors.

2. Materials and methods

The method to obtain DOI information presented in this study is described in section 2.1. A prototype module was produced and its performance evaluated in a two steps procedure. First, a standard characterization in terms of crystal separation, light output and energy resolution is performed by irradiating uniformly the module with a gamma source, in a configuration that reproduces the real working conditions of the array during a PET exam (section 2.4). Afterwards, the depth of interaction encoding capability is demonstrated by means of an electronic tagging setup, and DOI resolution is calculated for each crystal of the scintillator array (section 2.5). Finally, a preliminary investigation on timing performance is carried out (section 3).

2.1. Proposed method for DOI encoding

The method to obtain continuous DOI information proposed in this work is based on sharing and redirection of scintillation light among multiple detectors, together with attenuation of light over the length of the crystals by means of a mild depolishing of lateral sides of the scintillators. The concept is illustrated schematically in figure 1. When a gamma ray interacts

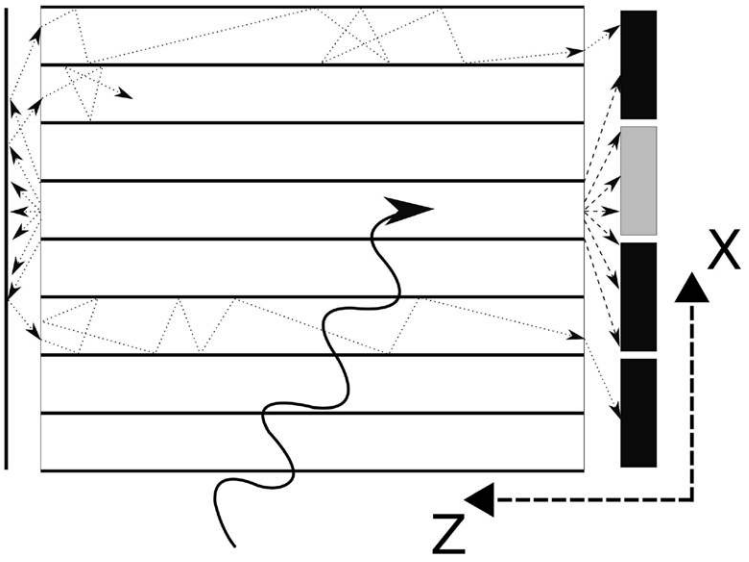

Figure 1. Schematic representation of the proposed DOI encoding method.

in a given point of a pixel in the scintillator array, the light produced propagates into the crystal and is eventually emitted both from the scintillator side coupled to the photodetector and from the opposite one (dashed and dotted arrows, respectively, in figure 1). It is well known that, because of the optical depolishing of the lateral surfaces of the crystal, the ratio of the amount of light at both ends depends on the gamma interaction position along the crystal (Vilardi *et al* 2006, Trummer *et al* 2009). For each scintillation event, the light emitted from the detector side of the crystal is spread over multiple detectors as an effect of the wide angular distribution of scintillation light. If the light collected by the ith detector is defined as p_i, and its physical position in a x–y plane is given by x_i and y_i, then the crystal of interaction can be reconstructed making use of a anger-logic scheme (Anger 1958) to compute the weighted average coordinates u and v

$$u = \frac{1}{P}\sum_{i}^{N} p_i x_i \qquad \text{and} \qquad v = \frac{1}{P}\sum_{i}^{N} p_i y_i \tag{1}$$

where N is the total number of detectors and P is the sum of the light collected by all the detectors

$$P = \sum_{i}^{N} p_i \tag{2}$$

The crystals can be separated by identifying the accumulation points in 2D scatter plots of the u,v coordinates. The detector collecting the maximum charge $p_{\max}$ is the one directly coupled to the crystal where the interaction occurred (grey), while the light emitted from the side of the crystal opposite to the detector and reflected back into the matrix by the mirror (black line) will spread over all the detectors. In this work we want to demonstrate how the ratio

$$w = \frac{p_{\max}}{P} \tag{3}$$

provides information about the depth of interaction z of the incident gamma ray.

Figure 2. Image of the prototype scintillator array produced by CPI Inc.

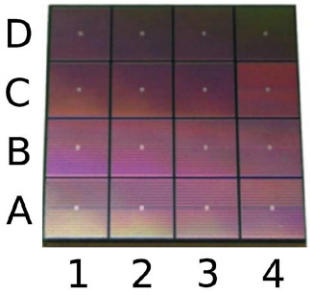

Figure 3. Image of the TSV MPPC array produced by Hamamatsu. The 16 detector channels of the array are labeled according to the legend shown on the picture.

2.2. Test module description

A scintillator array (figure 2) has been produced by Crystal Photonics Inc., United States, consisting in 64 LYSO crystals, each $1.53 \times 1.53 \times 15$ mm^3, arranged in a 8×8 array. Each 1.53×1.53 mm^2 face has been optically polished, while the remaining lateral faces are depolished. Foils of Enhanced Specular Reflector (ESR, by 3M), 70 μm thickness, inserted between the crystals, build the matrix structure, acting also as a wrapping material. The reflectors are not bonded to the scintillators, and therefore a thin air gap remains between ESR and crystals. The overall dimensions of the module array are $12.8 \times 12.8 \times 15$ mm^3, and the pitch between crystals is 1.6 mm. The entire module is then further wrapped with a layer of Teflon, to ensure mechanical stability. The photodetector (figure 3) is an Hamamatsu TSV MPPC array (S12642-0404PB-50), made of 16 SiPMs, each with 3×3 mm active area. The pitch between individual SiPMs is 3.2 mm. Each SiPM consists in 3464 single photon avalanche photodiodes (SPADs).

The scintillator matrix is coupled to the MPPC array by means of Rhodorsil 47 V optical grease. The alignment between matrix and MPPC is ensured by a 3D-printed plastic holder, and is such that 4 crystals are coupled to each individual SiPM. On the side of the matrix opposite to the crystals-MPPC interface, a piece of glass, $12.8 \times 12.8 \times 1$ mm^3, is inserted as a light guide between the matrix itself and a ESR foil. The light guide is coupled to the crystals with optical grease in order to maximize the extraction of light from the scintillators, while the interface between ESR and glass is in dry contact.

2.3. Reference module description

The mechanism of light redirection and attenuation described in section 2.1, besides allowing access to DOI information, is expected to affect the overall light output, energy resolution

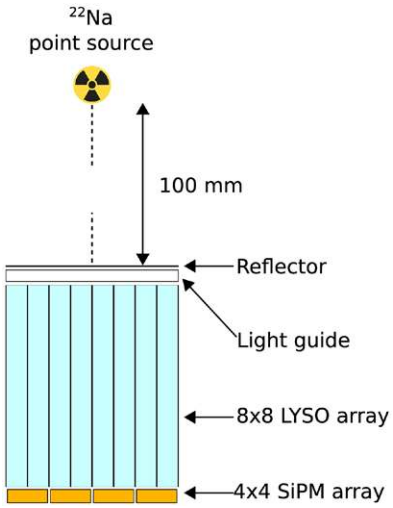

Figure 4. Schematic representation of the experimental setup used for standard characterization of the prototype module.

and timing resolution of the test module. In order to quantify these possible performance degradations, another scintillator array has been produced by Crystal Photonics Inc., United States, with the exact same geometry and structure of the test module, but with fully polished crystals. This reference module is coupled to the same Hamamatsu TSV MPPC array (S12642-0404PB-50) by means of Rhodorsil 47 V optical grease, and a ESR foil is used to cover the side of the matrix opposite to the crystals-MPPC interface, without the use of any light guide. The interface between ESR and crystal matrix is in dry contact.

2.4. PET-like experimental setup

The standard characterization of the module is performed by exciting the scintillators with a 3 MBq ^{22}Na source (1 mm active diameter) placed approximately 10 cm from the side of the matrix opposite to the MPPC, shown in figure 4. Readout of the MPPC array is performed through a 32-ch desktop digitizer by CAEN (model DT5740), connected to the MPPC detectors by a custom designed acquisition card that provides at the same time bias voltage to all the MPPC channels. The entire setup is contained in a light tight box, where temperature is kept constant at 20 °C by the cooling system.

Pulses are acquired in parallel whenever one of the channels exceeds a programmable threshold. For every trigger event, the charge collected by each of the input channels is recorded after pulse integration performed directly by the internal FPGA. All the channels of the MPPC array contribute to the generation of the trigger. Each event stored on the acquisition PC consists in a list of the 16 charges collected by the SiPMs. In a typical acquisition, a complete characterization can be carried out in about 15 min. The dataset stored on the acquisition PC contains scintillation events arising from any of the 64 crystals of the array. In order to perform a characterization of the test module on an individual crystal basis, a custom method (described in section 2.4.1) is applied to separate the contribution of each single scintillator. Finally, a charge spectrum is obtained for each crystal. In analogy with double side readout schemes adopted with depolished crystals, a proper charge spectrum can be reconstructed only by summing the light contributions emitted by both ends of the scintillator, which in this configuration corresponds to summing the charges collected by all the 16 SiPM detectors.

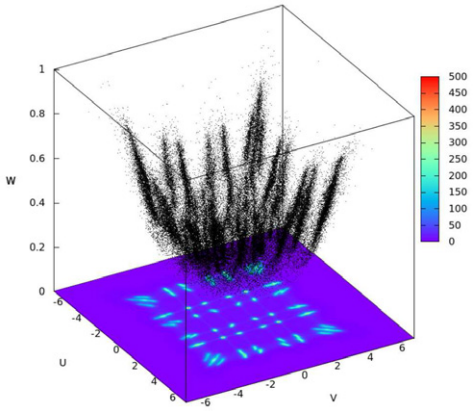

Figure 5. Three dimensional plot of the coordinates (u, v, w) for each event recorded in the PET-like acquisition. The projection of these events on the (u, v) plane is also shown.

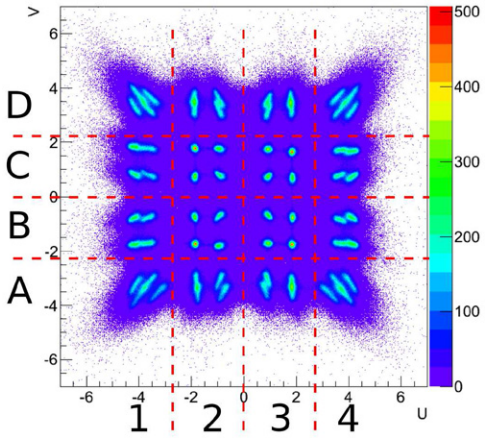

Figure 6. Two dimensional plot of the coordinates (u, v) for each event recorded in the PET-like acquisition. 16 groups of 4 crystals can clearly be identified and separated.

2.4.1. Crystal separation method. For a given acquisition dataset, a 3D graph of the (u, v, w) variables defined in equations (1) and (3) can be obtained, like the one shown in figure 5 along with its projection on the (u, v) plane. This plot shows 64 accumulation volumes, which, in analogy with standard 2D Anger logic, can be recognized as corresponding to the events for which an incident gamma ray has interacted with a single crystal of the scintillator matrix. Events for which energy has been deposited in multiple crystals, instead, are reconstructed far from these accumulation volumes and can be discarded since they would not be useful in a realistic PET system.

The 3D (u, v, w) points are projected on the (u, v) plane, as shown more in detail in figure 6. The dataset can then be divided into 16 separated areas, each corresponding to scintillation events localized into one group of 4 crystals directly coupled to a single SiPM. An example is shown in figure 7, where the (u, v, w) and (u, v) coordinates of events related to SiPM $A1$ (defined in figure 6) have been isolated by setting proper limits on the values of u and v.

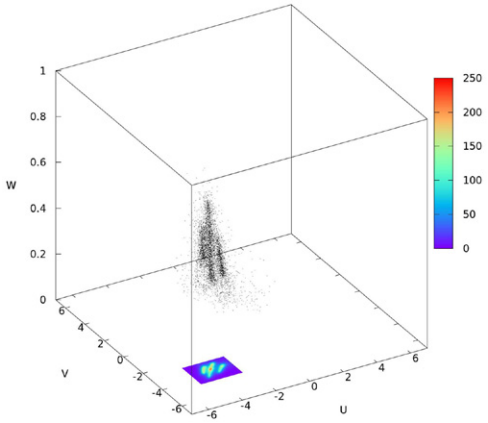

Figure 7. Three dimensional plot of the coordinates (u, v, w), and projection on (u, v) plane, of the events corresponding to SiPM A1.

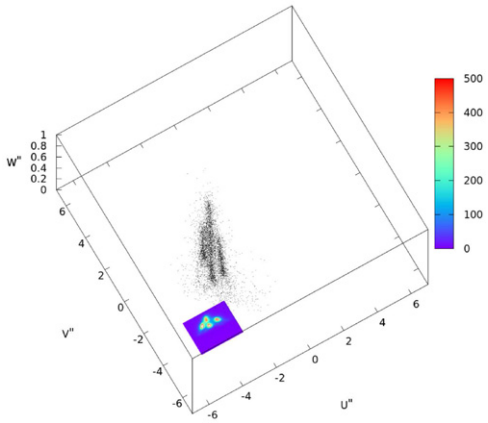

Figure 8. Three dimensional coordinate system is rotated and 3D points are projected on the new (u'', v'') plane, where they can be separated in 4 accumulation areas.

The (u, v, w) reference system is subsequently rotated by an angle θ around the w axis, and the resulting (u', v', w') system is further rotated by an angle ϕ around the v' axis. The angles θ and ϕ are chosen in such a way that, after the rotations, the main longitudinal axis of the four 3D accumulation volumes are as normal as possible to the plane (u'', v''). At this point, as shown in figure 8, the contribution of the scintillators can be separated into 4 spots by choosing appropriate boundary conditions on the variables u'' and v''. Finally, the procedure is repeated for each of the 16 SiPMs, and the events in the original dataset can be sorted among the 64 crystals of the scintillator array.

2.5. Electronic tagging setup

In order to demonstrate the possibility to obtain DOI information, an electronic tagging bench has also been developed. The module remains untouched on the same readout card used in the PET-like setup, which is sitting on a movable x–y–z stage. The the ^{22}Na source is placed on the lateral sides of the array, and aligned to a $1.5 \times 1.5 \times 15$ mm^3 LYSO tagging crystal

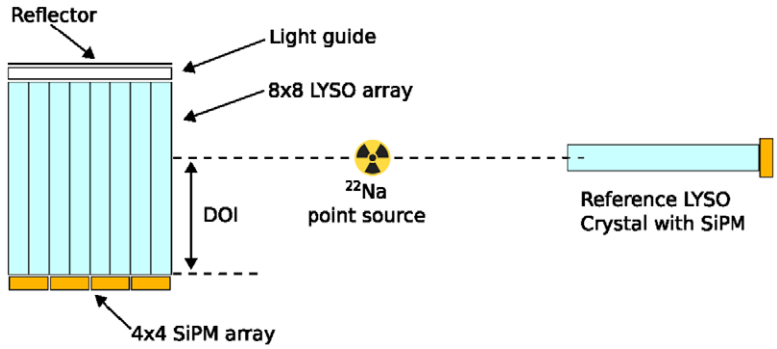

Figure 9. Schematic representation of the electronic tagging setup.

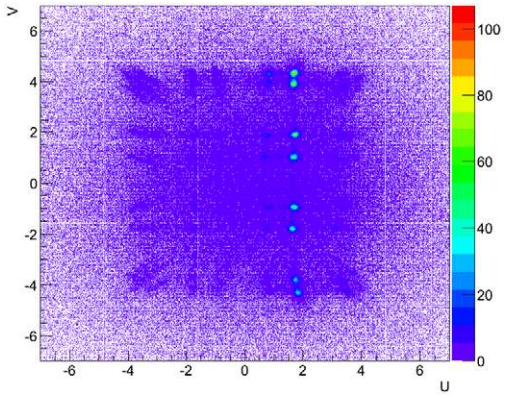

Figure 10. Two dimensional histogram of (u, v) coordinates for events acquired in a particular position with the electronic tagging setup.

glued to a single SiPM (see figure 9) connected to the CAEN desktop digitizer and acting as acquisition trigger.

When the signal on this detector exceeds a programmable threshold, the CAEN digitizer performs simultaneously the integration of the pulses recorded by the external SiPM and by all the 16 channels of the MPPC array. In this configuration, therefore, each event stored on the acquisition PC consists in a list of 17 charge values. Selecting photopeak events on the charge spectrum of the external SiPM restricts the dataset to scintillation events confined to a small excitation area of the crystal array. By means of the movable x–y–z stage, the entire matrix can be scanned in order to correlate the information extracted by the detectors to the incident gamma depth of interaction.

Monte Carlo simulations were performed by means of the Geant4 toolkit, in order to asses the size of the area excited by the electronic tagging setup. The FWHM size of the spot in the vertical direction (along the z axis in the frame of reference defined in figure 1) is on average 1.10 mm, and varies very slightly from the crystals belonging to the row closer to the ^{22}Na source with respect to the ones belonging to the furthest row. Based on this value, and in order to minimize the time required to characterize the entire scintillator array, it was decided to acquire data in 5 different vertical positions of the tagging setups, separated by 2.8 mm.

Once the detector is properly aligned and an acquisition is performed in a given z position, a flood map analogous to the one produced for the PET-like setup can be obtained.

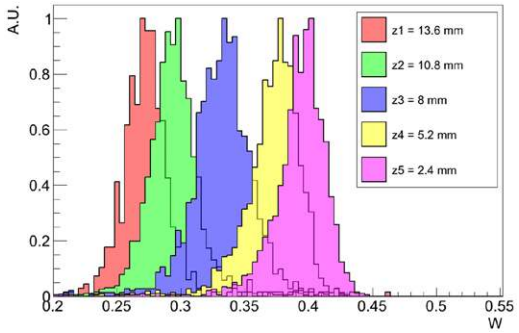

Figure 11. Histograms of the w variable for 5 z positions of the electronic tagging setup, for 511 KeV photoelectric events in a given crystal of the scintillator array. The value of z reported is the distance from the edge of the crystal that is coupled to the SiPM.

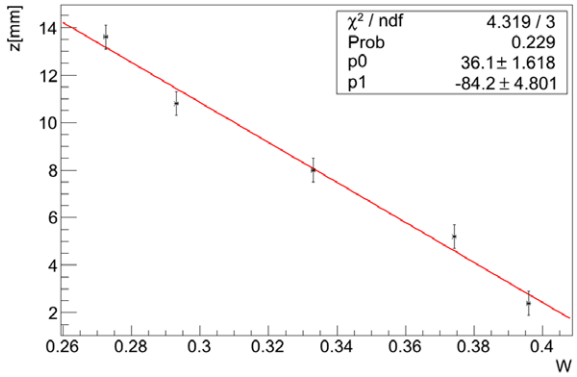

Figure 12. Correlation between the center of the irradiation spot defined by the z positions of the electronic tagging setup and the position of the corresponding w histogram peak, for a given crystal in the scintillator array.

An example is shown in figure 10. The 8 crystals irradiated can be separated by setting appropriate conditions on the (u, v) variables of this plot, a charge spectrum is derived, 511 KeV photopeak is selected, and the value of the w variable defined in equation (3) can be calculated from the measured signal amplitudes for all the pixels belonging to the same gamma interaction. The procedure is repeated for each the 5 positions of the vertical scan. The average value of w is found to move accordingly with the position of the tagging bench, as can been seen for one crystal in figure 11.

Figure 12 shows the correlation between the center of the irradiation spot (i.e. the vertical position of the tagging setup) and the peak position of w histograms, for one crystal in the scintillator array. Within the precision of our experimental setup, this correlation is linear and we can use a simple relation to describe it

$$z = m \cdot w + q \tag{4}$$

From this equation, the DOI resolution of a crystal can be derived as the uncertainty in reconstructing the real z position of an event, based on the value of w calculated for that event and the slope of the linear relation (4) for this particular crystal

$$\sigma(z) = m \cdot \sigma(w) \tag{5}$$

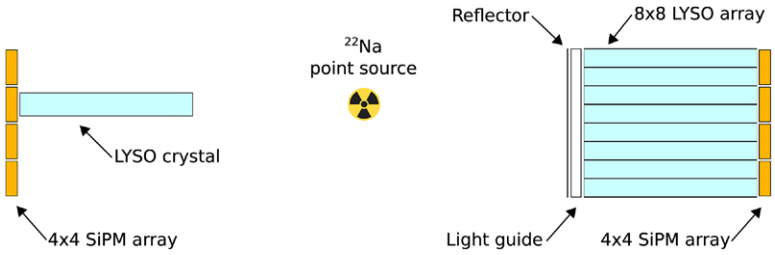

Figure 13. Schematic representation of the coincidence timing resolution setup.

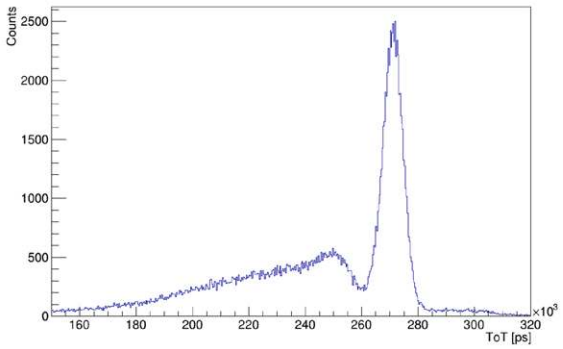

Figure 14. Typical time-over-threshold spectrum for the reference crystal.

3. Timing setup

We assessed the timing performance of the test module using a timing bench developed on the basis of the work previously carried out in our group to characterize the detector modules produced for the EndoTOFPET-US FP7 project (Auffray *et al* 2015). The bench is shown schematically in figure 13. A ^{22}Na source is placed halfway between the module and a single reference $3 \times 3 \times 15$ mm^3 LYSO crystal (Crystal Photonics Inc., United States), wrapped in ESR. The reference crystal is optically coupled to one SiPM of another Hamamatsu TSV MPPC array (S12642-0404PB-50), by means of Dow Corning RTV 3145. The signal of the SiPMs of both MPPCs is amplified and discriminated by NINO ASIC (Anghinolfi *et al* 2004) and sent to a high precision TDC (HPTDC—25 ps LSB) (Christiansen 2004). In order to minimize the time jitter introduced by the HPTDC, only the channel directly connected to the reference crystal and one channel on the MPPC of the test module are biased. In such a configuration, the crystal separation procedure described in section 2.4.1 cannot be performed and the contribution of the 4 crystals connected to the active SiPM cannot be separated. Time-over-threshold (ToT) spectra are obtained for the two channels in coincidence, as show in figure 14 and 15. Photoelectric events are selected from the ToT spectra and the time difference of the two channels is histogrammed in order to quantify the FWHM coincidence time resolution (CTR).

The contribution to CTR of the single reference crystal has been quantified by measuring on this setup the CTR resolution obtained between the reference crystal and another, identical $3 \times 3 \times 15$ mm^3 LYSO crystal from the same producer. The value found, 219 ± 4 ps FWHM, has been divided by $\sqrt{2}$ to get the reference crystal timing resolution of 155 ± 3 ps FWHM. The contribution of the reference crystal is then subtracted from the CTR values obtained by

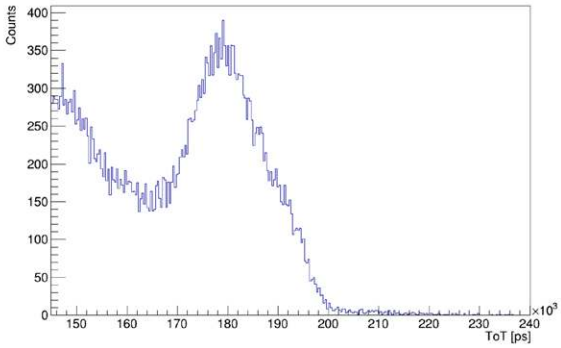

Figure 15. Typical time-over-threshold spectrum for one SiPM channel of the MPPC array.

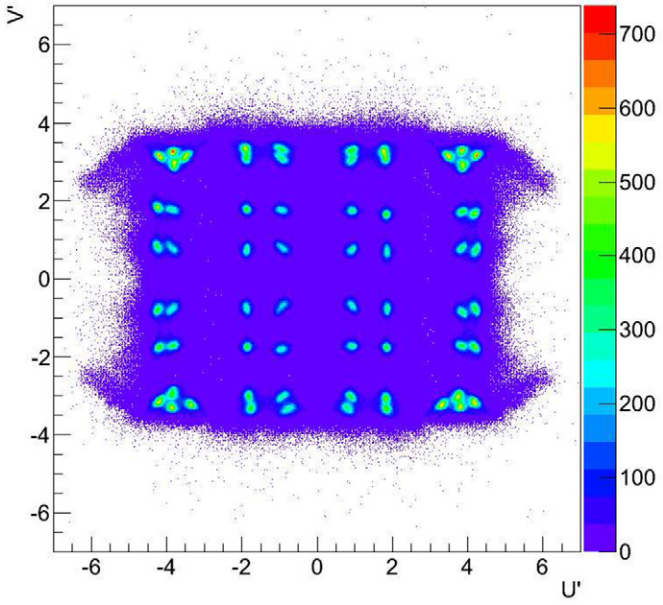

Figure 16. Two dimensional histogram showing the separation of all the 64 crystals in the scintillator array.

the timing setup, in order to get the single module timing resolution. The CTR of two identical modules is then derived by multiplying this value by $\sqrt{2}$.

4. Results

The performance of the prototype module is evaluated on a crystal by crystal basis. In a realistic PET scanner, several modules like the one described in this paper would be used to build each of the detector plates. The light sharing and redirection mechanism described in section 2.1 would involve the entire array of modules, rather than just one. In such a configuration, the majority of the crystals would effectively be in the same conditions of the 16 crystals

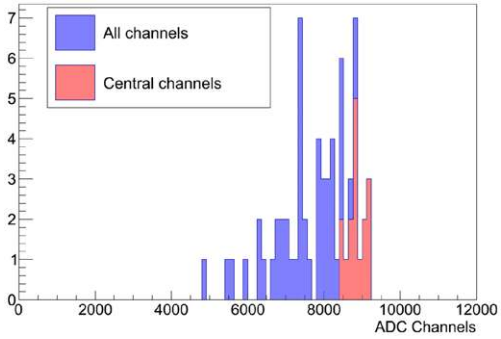

Figure 17. Distribution of 511 KeV photopeak positions for all the 64 crystals in the scintillator array (blue) and for the 16 crystal coupled to the 4 central SiPMs (red).

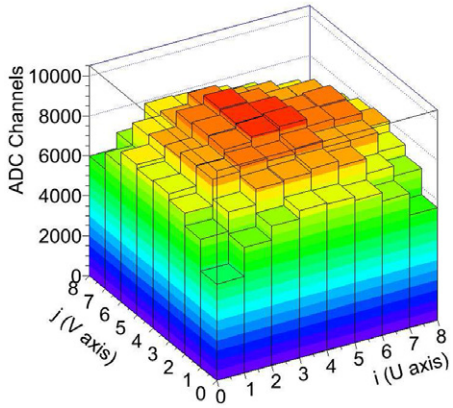

Figure 18. Spatial distribution of 511 KeV photopeak positions for all the 64 crystals in the scintillator array.

coupled to the 4 central SiPMs in our prototype. In the following discussion the performance of these 16 crystals will be therefore highlighted.

4.1. Crystal separation

Good crystal separation can be obtained for all the 64 crystals of the scintillator array, as shown in figure 16. The dataset can therefore be divided into contributions arising from scintillation events localized in individual crystals, by setting appropriate limits on the values the variables (u'', v'') defined in section 2.4.1. By restricting the analysis to these events, scattering between multiple scintillators are discarded.

While the separation capability of the module is excellent for the 16 crystals coupled to the 4 central SiPMs, it becomes less efficient for the scintillators closer to the edge of the module. This can be easily explained by considering that the algorithm described by equations (1) relies on the knowledge of light distribution around the channel under study. For the channels on the edge of the module, the lack of a complete ring of detectors surrounding the channel leads to a decreased efficiency of the algorithm. Anyway, crystal separation is still possible.

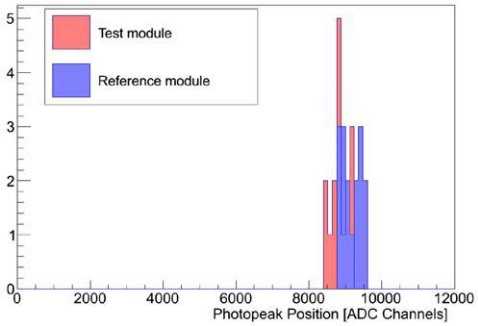

Figure 19. Light output of the 16 central crystals of the prototype module (red) compared to a reference polished module (blue).

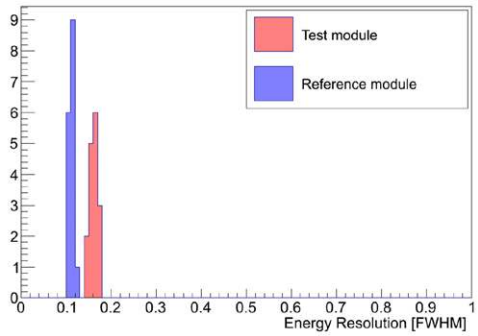

Figure 20. Energy resolution FWHM of the 16 central crystals of the prototype module (red) compared to a reference polished module (blue).

4.2. Light output and energy resolution

After crystal separation, all the 64 charge spectra of the scintillators in the array can be obtained and both the 511 KeV and 1275 KeV photoelectric peaks can be recognized. In figure 17 the distribution of 511 KeV photopeak positions for all the 64 scintillators is shown, highlighting in red color the contribution of the 16 crystals coupled to the 4 central SiPMs of the detector array. The total light collected becomes lower as the crystal position gets closer to the edge of the scintillator array, as can be seen also in figure 18. This effect can be explained by light leakage through the lateral surfaces of the glass light guide placed on the side of the scintillator array opposite to the photodetector. The closer the crystal is to the edge of the matrix, in fact, the larger is the portion of light emitted by its rear face that hits these surfaces with an angle favourable to allow transmission to the air surrounding the module.

The light output of the 16 central crystals has been compared to the output of scintillators in the same position of the reference module described in section 2.3. This comparison is shown in figure 19. For the test module, an average of 8800 ± 200 ADC channels was found, while for the reference module 9100 ± 200 ADC channels.

Concerning energy resolution, the distributions for the test matrix are shown in figures 21 and 22, while the comparison with the reference matrix can be found in figure 20. On average, the 16 crystals coupled to the 4 central SiPMs of the test matrix show an energy resolution FWHM of $16.1\% \pm 0.6\%$. This value is significantly different from the average

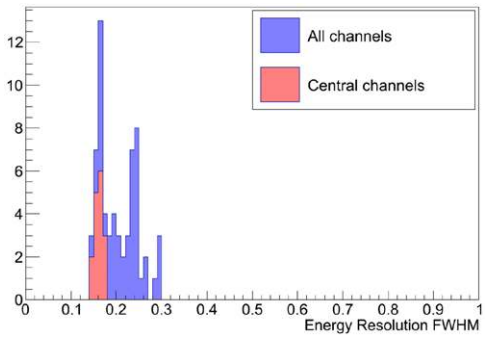

Figure 21. Distribution of 511 KeV FWHM energy resolution for all the 64 crystals in the scintillator array (blue) and for the 16 crystal coupled to the 4 central SiPMs (red).

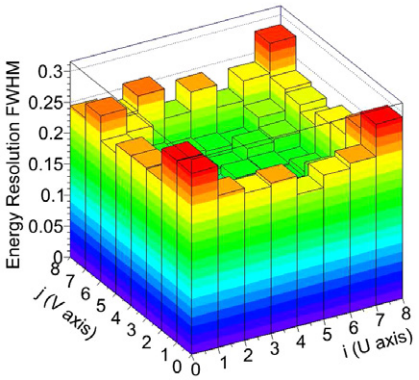

Figure 22. Spatial distribution of 511 KeV FWHM energy resolutions for all the 64 crystals in the scintillator array.

of $11.2\% \pm 0.3\%$ found for the reference matrix, and can be explained by a combination of the effect of depolishing and the increased light absorption due to the presence of the light guide.

4.3. Depth of interaction

All the crystals of the scintillator array have been scanned with the electronic tagging setup. A linear relation between the values of w calculated for scintillation events and the position of the excitation spot was found for all the scintillators. We can therefore confirm the initial hypothesis that the method proposed in this paper is capable of providing continuous DOI information with a single side readout scheme. The DOI resolution has also been quantified, and an average value of 4.1 ± 0.1 mm FWHM has been found, as shown in figure 23. The DOI resolution, within the precision of our characterization bench, does not seem to have a dependence on the position of the crystal in the array (see figure 24).

4.4. Energy resolution correction

Given the linear relation between the w variable and the position of gamma excitation along the main crystal axis, it is possible to apply a correction, event by event, to the total charge

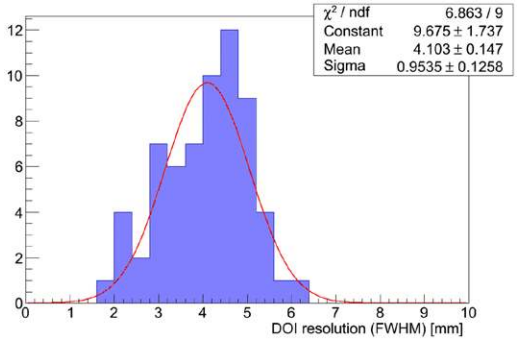

Figure 23. Distribution of FWHM DOI resolution for all the 64 crystals in the scintillator array.

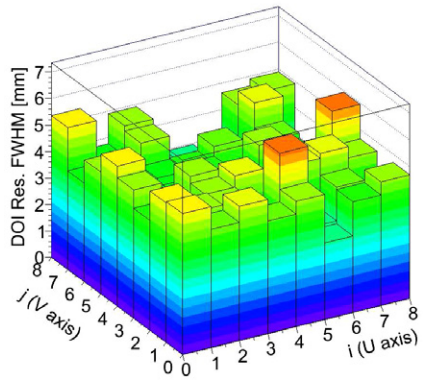

Figure 24. Spatial distribution of FWHM DOI resolution for all the 64 crystals in the scintillator array.

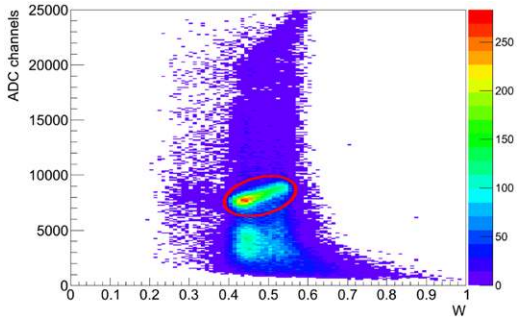

Figure 25. Scatter plot of the total energy collected by the 16 SiPMs versus the *w* variable for a crystal in the scintillator matrix. The 511 KeV photopeak events are highlighted in red.

collected by the 16 SiPMs in order to improve the energy resolution of the module. For each crystal, a scatter plot of the total energy collected versus *w* is produced, like the one shown in figure 25. The area of photoelectric events is isolated, then divided in slices parallel to the vertical axis.

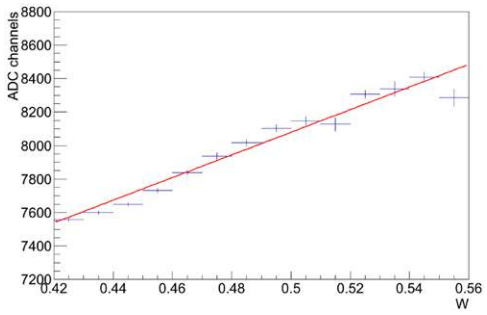

Figure 26. Correlation between peak position and w variable for a crystal in the scintillator array.

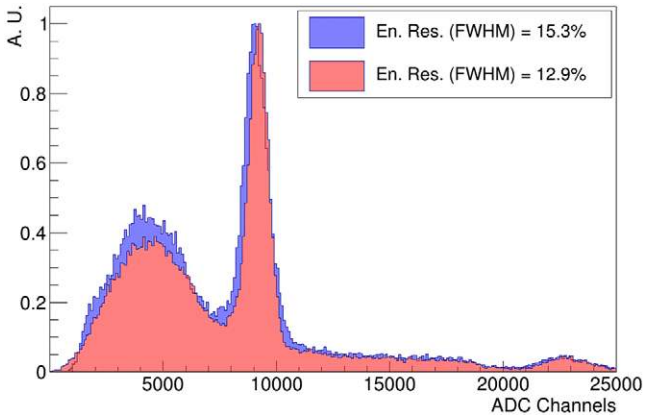

Figure 27. Comparison between a standard charge spectrum (blue) and the same dataset corrected using the DOI information derived by w (red) for one crystal of the array.

The peak position of each slice is found by means of Gaussian fitting, then plotted against the corresponding w position, as shown in figure 26. A linear relation is derived by this plot and it is used to correct, event by event, the value of total charge collected by the 16 SiPMs, and a corrected charge spectrum is produced. As shown by the comparison between the uncorrected and corrected spectra of a sample crystal in figure 27, the width of the 511 KeV photoelectric peak is reduced and the energy resolution therefore improved.

Distributions of the corrected energy resolutions for all the 64 scintillators in the test matrix can be found in figure 28 and 29. For the 16 crystals coupled to the 4 central SiPMs of the test matrix the average energy resolution FWHM is improved from the $16.1\% \pm 0.6\%$ value previously found to $12.7\% \pm 0.2\%$.

5. Timing resolution

Timing resolution has been measured for both the test and reference modules, for the 4 central SiPMs of the MPPC array. On average the CTR of two test modules in coincidence is evaluated in 428 ± 8 ps FWHM. This value is consistently different from the CTR of 321 ± 6 ps FWHM obtained on the same bench for the reference module. However, the

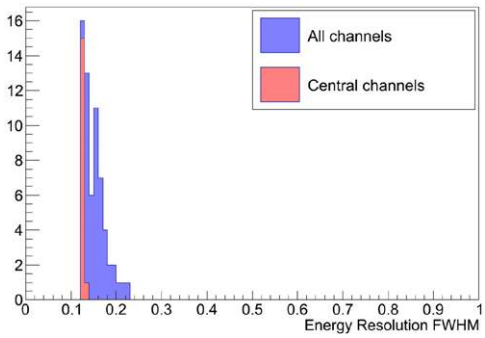

Figure 28. Distribution of 511 KeV FWHM energy resolution, corrected by DOI, for all the 64 crystals in the scintillator array (blue) and for the 16 crystal coupled to the 4 central SiPMs (red).

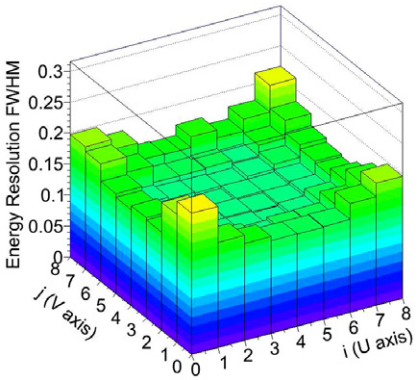

Figure 29. Spatial distribution of 511 KeV FWHM energy resolutions, corrected by DOI, for all the 64 crystals in the scintillator array.

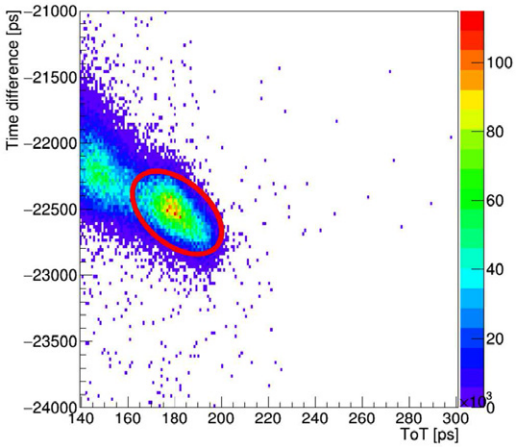

Figure 30. Scatter plot of the time difference between reference crystal and test module and ToT, for a single channel of the MPPC array. The 511 KeV photopeak events are highlighted in red.

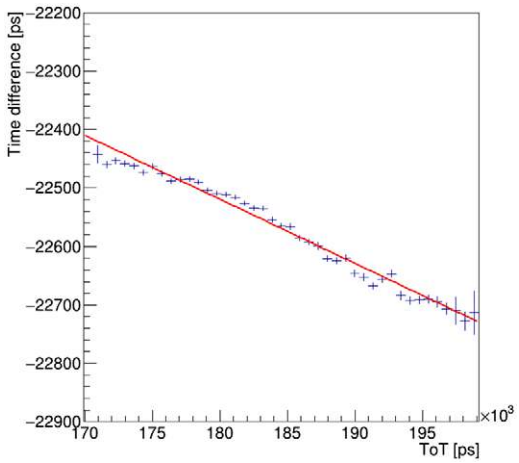

Figure 31. Correlation between the time difference between reference crystal and test module and ToT, for a single channel of the MPPC array.

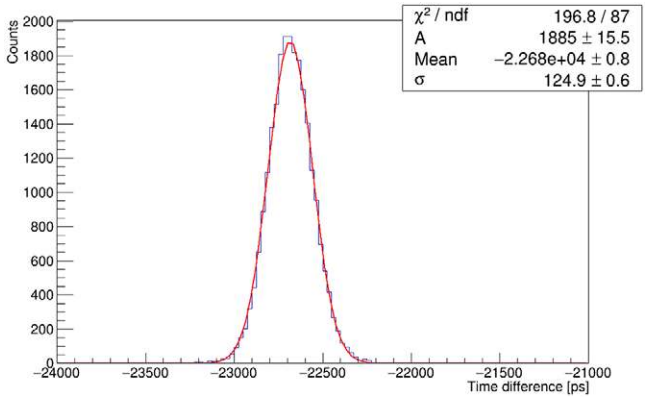

Figure 32. Distribution of time difference between reference crystal and test module, for a single channel of the MPPC array.

test module allows access to the additional information of the DOI of incident gammas, and this information can be used to correct for the spread in photon travel times caused by scintillation events localized in different areas of the same crystal. The fraction of light, and therefore the ToT, recorded by the SiPM coupled to the crystal where the gamma is interacting is linearly correlated to the DOI, as demonstrated in section 4.3. When photoelectric events are selected in the spectrum of the test module, if their ToT is plotted against the time difference of the two channels, a clear correlation can be spotted, as shown in figure 30. It has to be noted that no such a correlation was found for the reference module. A linear relation can be derived, as show for one channel in figure 31, and used to correct, event by event, the values of time difference between the reference crystal and the test module. By applying this correction, the CTR of two identical test modules can be estimated in 353 ± 7 ps FWHM, with a degradation of about 30 ps compared to the reference module, as shown in figure 32.

6. Discussion

The continuous DOI encoding capability of the method proposed in this work has been demonstrated, with an average DOI resolution for the prototype module evaluated in 4.1 ± 0.1 mm FWHM over 15 mm long crystals. The resolution has been shown to be homogeneous along the length of the crystals, within the experimental precision of our setup. Furthermore, no consistent deterioration of the DOI resolution has been found for the crystals on the edge of the array. Pixel separation is excellent for the crystals coupled to the 4 central MPPCs, while some degradation can be noted for the pixels located at the edge of the matrix. Light losses were found to be negligible as compared to a matrix with the same dimensions and structure made of fully polished crystals and without any glass light guide. The energy resolution, after applying a correction based on the DOI information, was evaluated in $12.7\% \pm 0.2\%$ FWHM at 511 KeV. Preliminary evaluation of the timing resolution of the module has been carried out. The coincidence timing resolution was estimated in 353 ± 7 ps FWHM, with a degradation of about 30 ps when compared to an identical module with polished crystals and no glass light guide.

The method proposed represents a competitive solution for designing PET scanners with DOI encoding capability. The DOI resolution achieved is in fact comparable to what has been reported by exploiting the light sharing through triangular teeth shaped reflectors separating the individual scintillators (Ito *et al* 2013), while it is consistently better as compared to solutions adopting light sharing through an ESR reflector (Yang *et al* 2009) or light sharing among multiple layers of crystals arranged in offsetted positions (Ito *et al* 2010). Better DOI resolution has been found for double side G-APD cross-strip readout (Kolb *et al* 2014), but with worse timing resolution. Phosphor coated scintillators also show better DOI resolution (Berg *et al* 2016), but at the same time perform worse in terms of both energy and timing resolution. Monolithic-crystal PET detectors have shown better DOI resolution with double side readout, while single side readout has shown similar performance (Peet *et al* 2015).

7. Conclusions

A new method for DOI determination in PET scanners with single side readout and depolished crystals has been developed and validated. The performances shown by the prototype module, in combination with the adoption of single side readout and 4-to-1 crystal-SiPM coupling, suggest that the method proposed in this study can effectively be adopted to develop high resolution PET scanners while keeping the overall complexity of the systems to a reasonably low level.

Acknowledgments

This work has been carried out in the frame of the Crystal Clear Collaboration, under the Contract Agreement KM2912/KT/PH/004C, and partially supported by a Marie-Curie Early Initial Training Network Fellowship of the European Community's 7th Framework Program under Grant Agreement (PITN-GA-2011-289355- PicoSEC-MCNet). The authors would like to thank Katayoun Doroud for the development of the acquisition card and Dominique Deyrail for the help in the setup of the experimental benches.

References

Anger H O 1958 Scintillation camera *Rev. Sci. Instrum.* **29** 27–33

Anghinolfi F, Jarron P, Martemyanov A N, Usenko E, Wenninger H, Williams M C S and Zichichi A 2004 NINO: an ultra-fast and low-power front-end amplifier/discriminator ASIC designed for the multigap resistive plate chamber *Nucl. Instrum. Methods* A **533** 183–7

Auffray E *et al* 2015 Characterization studies of silicon photomultipliers and crystals matrices for a novel time of flight pet detector *J. Instrum.* **10** P06009

Berg E, Roncali E, Kapusta M, Du J and Cherry S R 2016 A combined time-of-flight and depth-of-interaction detector for total-body positron emission tomography *Med. Phys.* **43** 939–50

Bugalho R *et al* 2009 Experimental characterization of the Clear-PEM scanner spectrometric performance *J. Instrum.* **4** P10011

Christiansen J 2004 HPTDC high performance time to digital converter *Technical Report* CERN Geneva Version 22 for HPTDC version 13 (https://cds.cern.ch/record/1067476/files/cer-002723234.pdf)

Ito M, Lee J S, Kwon S I, Lee G S, Hong B, Lee K S, Sim K S, Lee S J, Rhee J T and Hong S J 2010 A four-layer DOI detector with a relative offset for use in an animal PET system *IEEE Trans. Nucl. Sci.* **57** 976–81

Ito M, Lee M S and Lee J S 2013 Continuous depth-of-interaction measurement in a single-layer pixelated crystal array using a single-ended readout *Phys. Med. Biol.* **58** 1269

Kang H G, Ko G B, Rhee J T, Kim K M, Lee J S and Hong S J 2015 A dual-ended readout detector using a meantime method for sipm tof-doi pet *IEEE Trans. Nucl. Sci.* **62** 1935–43

Karp J S and Daube-Witherspoon M E 1987 Depth-of-interaction determination in NaI(TL) and BGO scintillation crystals using a temperature gradient *Nucl. Instrum. Methods Phys. Res.* A **260** 509–17

Kolb A, Parl C, Mantlik F, Liu C C, Lorenz E, Renker D and Pichler B J 2014 Development of a novel depth of interaction PET detector using highly multiplexed G-APD cross-strip encoding *Med. Phys.* **41** 081916

Levin C 2002 Design of a high-resolution and high-sensitivity scintillation crystal array for PET with nearly complete light collection *IEEE Trans. Nucl. Sci.* **49** 2236–43

Liu H, Omura T, Watanabe M and Yamashita T 2001 Development of a depth of interaction detector for γ-rays *Nucl. Instrum. Methods Phys. Res.* A **459** 182–90

Miyaoka R S, Lewellen T K, Yu H and McDaniel D L 1998 Design of a depth of interaction (DOI) PET detector module *IEEE Trans. Nucl. Sci.* **45** 1069–73

Peet B J, Borghi G, Tabacchini V and Schaart D 2015 Millimeter spatial resolution and sub-200 ps timing in 32 mm $\times$ 32 mm $\times$ 22 mm monolithic lyso: Ce crystals with dual-sided digital photon counter readout *J. Nucl. Med.* **56** 602

Seifert S and Schaart D R 2015 Improving the time resolution of TOF-PET detectors by double-sided readout *IEEE Trans. Nucl. Sci.* **62** 3–11

Trummer J, Auffray E and Lecoq P 2009 Depth of interaction resolution of LuAP and LYSO crystals *Nucl. Instrum. Methods Phys. Res.* A **599** 264–9

Vilardi I *et al* 2006 Optimization of the effective light attenuation length of YAP:Ce and LYSO: Ce crystals for a novel geometrical PET concept *Nucl. Instrum. Methods Phys. Res.* A **564** 506–14

Wiener R, Surti S and Karp J 2013 DOI determination by rise time discrimination in single-ended readout for TOF PET imaging *IEEE Trans. Nucl. Sci.* **60** 1478–86

Yang Y, Wu Y and Cherry S R 2009 Investigation of depth of interaction encoding for a pixelated LSO array with a single multi-channel PMT *IEEE Trans. Nucl. Sci.* **56** 2594–9